COBEM 2021 26th International Congress of Mechanical Engineering
November 22-26, 2021, Virtual Congress, Brazil

# COB-2021-0051
# EXPERIMENTAL CHARACTERIZATION AND COMPUTATIONAL MODELLING OF THE EFFECT OF IN VITRO CORROSION ON THE MECHANICAL INTEGRITY OF BIODEGRADABLE MAGNESIUM ALLOY WE43 FOR ORTHOPEDIC APPLICATIONS

**Felipe Saconi**
Aeronautical Engineering Department / São Carlos School of Engineering / University of São Paulo - Av. João Dagnone, 1100 - Jardim Santa Angelina - São Carlos, SP, Brasil - 13563-120
felipe.saconi@usp.br

**Anish Roy**
Wolfson School of Mechanical, Electrical and Manufacturing Engineering / Loughborough University , Leicestershire, LE11 3TU, UK
a.roy3@lboro.ac.uk

**Marcelo Leite Ribeiro**
Aeronautical Engineering Department / São Carlos School of Engineering / University of São Paulo - Av. João Dagnone, 1100 - Jardim Santa Angelina - São Carlos, SP, Brasil - 13563-120
malribei@usp.br

***Abstract.*** *Biodegradable magnesium alloys are considered a promising candidate to replace the conventional bioinert metals, such as titanium alloys, used in trauma and extremities implants. Nowadays, large-scale utilization of magnesium implants is still restricted by the high corrosion rates and its unknown effects on implant structural integrity. Computational modeling plays an important role in the development and design of orthopedic implants for osteosynthesis. In the case of biodegradable metals, a modelling approach is required to predict the effects of degradation on the implant's mechanical integrity and its capacity to provide the desired stabilization of fractured bones. In this study, the mechanical behavior of magnesium WE43 alloy is modelled using the von Mises elastoplasticity model with isotropic hardening, coupled with a continuum damage mechanics model, to accounts for the effects of corrosion-induced microscale defects on the material mechanical resistance. The phenomenological corrosion model is implemented in a finite element framework, through the development of a user material subroutine (VUMAT) for use with the Abaqus/Explicit. The corrosion damage is assumed to be nonuniform, also known as localized pitting corrosion, which represents the heterogeneous corrosion on the materials free surface when exposed to an aggressive environment, as well as stress corrosion, which describes the stress-mediated localization of the corrosion attack through a stress-dependent evolution law. Both pitting and stress corrosion damages are implemented employing a nonlocal integral formulation, in order to overcome the mesh-dependency. The nonlocal pitting corrosion model is calibrated based on experimental data collected from in-vitro degradation experiments and mechanical testing of magnesium WE43 alloy wire specimens. The calibrated corrosion model accurately captures both the mechanical reduction in specimen resistance, in the form of failure strength with mass loss, as well as the non-linear corrosion behavior of magnesium WE43, observed experimentally.*

***Keywords:*** *magnesium alloy, numerical simulation, continuum damage mechanics, pitting corrosion modelling, finite element analysis.*

## 1. INTRODUCTION

Biodegradable magnesium alloys are considered a promising candidate to replace the conventional bioinert metals, such as titanium alloys and stainless steel, used in trauma and extremities implants (Waizy *et al.*, 2014). Magnesium alloys are totally biodegradable in the human body, making a second surgery for implant removal unnecessary. Additionally, they present osteoconductive properties, which contributes to bone healing (Staiger *et al.*, 2006). Regarding mechanical properties, Mg alloys have an elastic modulus similar to that of bone, 35-45GPa, which helps to prevent the stress shielding effect, while possessing sufficient mechanical strength to be used in load bearing applications. Among different alloys that are been researched for orthopedic applications, the WE43 magnesium alloy has gained great attention, since it was the first magnesium alloy approved for human use, under the commercial name Magnezix® (Seitz

*et al.*, 2016). The WE43 magnesium alloy belongs to the Mg-Y-RE-Zr system, containing nominally 4 wt % Y, 3 wt % rare earths, and 0.5 wt % Zr (Griebel *et al.*, 2018).

The biodegradability of Mg alloys is related to its corrosion process. The corrosion behavior of Mg alloys is driven by different factors, such as: alloy composition, material processing, superficial finishing, corrosion environment, as well as load conditions (Grogan, 2013). According to Song and Atrens (2003), the Mg corrosion process in neutral aqueous environment occurs by an electrochemical reaction with water to produce magnesium hydroxide and hydrogen gas. The overall reaction for the corrosion of Mg is shown in Eq. (1). The magnesium hydroxide forms a protective layer on materials surface. However, in physiological environments, rich in chloride solutions, this protective layer is broken down, according to Eq. (2), leading to further corrosion.

$$Mg + 2\,H_2O \rightarrow Mg(OH)_2 + H_2, \tag{1}$$

$$Mg(OH)_2 + 2\,Cl^- \rightarrow MgCl_2\,, \tag{2}$$

Magnesium and its alloys are susceptible to different corrosion mechanisms: microgalvanic corrosion, localized pitting corrosion, stress cracking corrosion and fatigue corrosion (Gastaldi *et al.*, 2011). The microgalvanic corrosion is related to different electrochemical potential between the Mg, which acts as an anode, and second phases or impurity phases, which acts as the cathode, resulting in highly localized corrosion. The localized pitting corrosion is related to the breakage of material passivation layer when exposed to aggressive physiological environment, rich in chloride solutions, which starts as irregular pits that spread laterally and cover the whole surface. Lastly, the stress cracking corrosion involves the interaction between the material, the environment and the applied stress, and can be either intergranular, related to cracks formation and propagation due to the localized corrosion defects, as well as transgranular, related to cracks formation and propagation due to hydrogen embrittlement (AgarwaL *et al.*, 2016; Atrens *et al.*, 2011; Gastaldi *et al.*, 2011; Song and Atrens, 2003).

Nowadays, large-scale utilization of magnesium implants is still restricted by the high corrosion rates and its unknown effects on material structural integrity. The most common mean of assessing the effects of degradation on material structural integrity is performing experimental testing, which can be very costly, financially and time wise. In addition to experimental testing, computational modeling of the corrosion process can be an efficient tool on the understanding of corrosion effects, thus playing an important role in the development and in the design optimization of orthopedic implants. In the literature, different authors have used a phenomenological-based continuum damage mechanics (CDM) approach for predicting the performance of biodegradable materials. Gastaldi *et al.* (2011) developed a multi mechanism corrosion model within the framework of CDM to simulate both uniform and stress corrosion of magnesium alloys for coronary stent applications. Grogan *et al.* (2011) extended the uniform corrosion model proposed by Gastaldi *et al.* (2011) in order to account for the localized pitting corrosion mechanism present in most biodegradable magnesium alloys. As these models are phenomenological-based, they evaluate the material corrosion damage by means of arbitrary state variables, which progressively degrades the mesh elements, without explicit modeling the corrosion phenomena and their evolution, in other words, it does not capture physical and chemical processes responsible for causing the corrosion, such as electrochemical surface reactions.

The main objective of this work is to implement a phenomenological multi mechanism corrosion model, based on CDM theory, to be used in future research on the design of orthopedic implants, for example, pins, screws and plates. The secondary objective of this work includes the experimental characterization of both mechanical and in vitro degradation behavior of magnesium WE43 alloy wires for finite element model calibration.

## 2. MATERIALS AND METHODS

### 2.1 Sample

Mg WE43 alloy wires, with diameters of 0.84 mm, were produced by Meotec GmbH, Germany, and sourced from FortWayne Metals, USA, with 40% of cold work. The wire was subsequently cut into different length samples for mechanical characterization and corrosion testing.

### 2.2 Mechanical characterization

The real stress-strain curve from the uniaxial tension test was used to identify the plastic hardening behavior of WE43 magnesium alloy, including Modulus of Elasticity, Yield Strength and the Ultimate Tensile Strength (UTS). The material was tested in two different thermomechanical conditions: as drawn, with no thermal treatment, and annealed at 400ºC (Maier *et al.*, 2015). Samples for tensile tests had a total length of 84mm, with a grip span of 50mm. A MTS Bionix Servohydraulic Test System tensile testing machine, with a 15 kN load cell, was used for mechanical characterization. The tensile testing was conduct at a constant test velocity equal to 1 mm/min. Data was collect using the TestWorks 4, at a 1 Hz frequency, and analyzed using the Minitab 17 software.

### 2.3 Corrosion testing

In order to characterize the in vitro degradation behavior of the WE43 alloy, two independent corrosion experiments were carried out.

The first corrosion experiment was realized to characterize the corrosion rate of Mg WE43 in simulated body fluid (SBF). The Mg WE43 alloy corrosion rate was determined using the hydrogen gas evolution method proposed by Song *et al.* (2001). This method relays on the set up shown in Figure 1 to collect and to measure the volume of gas released from each sample due to corrosion process. Further, the volume of gas released from each sample was used along magnesium corrosion chemical equations to calculated the corrosion rate. In this experiment, three samples, length = 30mm, were exposed to corrosion for a period of 168h. The hydrogen evolution technique allows dynamical and instantaneous determination of corrosion rate and has shown high correlation with the direct mass loss weighting technique, Kirkland *et al.* (2012).

The second corrosion experiment was realized to quantify the corrosion effect on the material's structural integrity. This was done by corroding 24 specimens, with the same dimensions of the specimens used in "Mechanical characterization" section, for different time periods. A PTFE (Polytetrafluoroethylene) coating was applied on the extremities of the specimens, leaving only the 50mm grip span region exposed to corrosion. After degradation, the specimens were removed from corrosion electrolyte, cleaned in chromic acid 20% and tested in uniaxial tension until fracture, following the same methodology used in the "Mechanical characterization" section.

The annealed condition was chosen for corrosion experiments 1 and 2. For both corrosion experiments, specimens were subjected to thermal treatment, cleaned with chromic acid 20%, rinsed with distilled water, and left to dry in the oven at 65 ºC for a period of 1h, in order to achieve consistent surface oxidation. The conventional SBF (c-SBF), prepared according to Oyane *et al.* (2002), at a body temperature of 36.5 ºC was adopted as corrosion electrolyte. An electrolyte volume (ml) to corrosion area ($cm^2$) ratio greater than 50:1 was adopted for both experiments. This ratio is much larger than the critical ratio of 6.7 found by Yang and Zhang (2009).

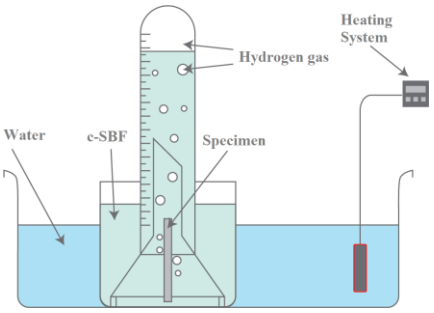


Figure 1- Hydrogen gas evolution method set up.

### 2.4 Model overview

A Finite Element (FE) framework based on continuum damage mechanics (CDM) theory was implemented to phenomenologically simulate the influence of corrosion on the mechanical behavior of biodegradable magnesium alloys. The corrosion damage framework is implemented via the FORTRAN user material subroutine, or VUMAT, in the FE solver Abaqus/Explicit (Dassault Systèmes, Waltham, MA, USA). Abaqus/Explicit has an interface that allows the user to implement the constitutive relationships of any given arbitrary complexity beyond the existing material models present in Abaqus material library.

The use of CDM theory allows the effects of corrosion-induced mas loss and microscale defects on overall material structural integrity to be accounted for. This is achieved through the implementation of a corrosion parameter, $D$, representing the magnitude of damage and an effective stress tensor, $\tilde{\sigma}_{ij}$ as described by Lemaitre (1985). The effective stress tensor is given by Eq. (3):

$$\tilde{\sigma}_{ij} = \frac{\sigma_{ij}}{1-D}, \tag{3}$$

where $\sigma_{ij}$ is the Cauchy stress tensor and $D$ is the corrosion parameter ($(0 \leq D \leq 1)$, where $D \approx 1$ represents the element fully damaged state.

In the present work, corrosion of WE43 alloy is assumed to be a superposition of two types of non-uniform corrosion processes: pitting corrosion ($D_p$) and stress corrosion ($D_{sc}$). The contributions due to both pitting and stress corrosion are superposed linearly, according to the proportionality parameter $f$, in order to evaluate the overall damage parameter $D$:

$$D = (1 - f)D_p + (f)D_{sc}, \tag{4}$$

Both pitting corrosion ($D_p$) and stress-driven corrosion ($D_{sc}$) are implemented using a nonlocal integral formulation to overcome the mesh size dependency, intrinsic to the continuum damage mechanics approach (Ma *et al.*, 2018). For the pitting corrosion only model, the proportionality parameter assumes the value of $f = 0$.

The pitting corrosion model is implemented using a nonlocal integral formulation as proposed by Ma *et al.* (2018) based on the previous works of Grogan *et al.* (2011) and Fathi *et al.* (2017). The evolution law of the pitting corrosion damage parameter is defined as:

$$\frac{dD_p}{dt} = \lambda_e^* k_p, \tag{5}$$

where $k_p$ is the corrosion kinetic parameter, in units of $\mathrm{h}^{-1}$, which requires calibration based on experimental data, and $\lambda_e^*$ is a non-local averaging pitting parameter of a material point with the position vector **x**, which is calculated as:

$$\lambda_e^*(x) = \int_V \alpha(x,y)\, \lambda_e\,(y) dV, \tag{6}$$

where $\lambda_e$ is the local pitting parameter of a material point with the position vector **y** in the influencing zone of the material point **x** and $\alpha(x,y)$ is the nonlocal average operator defined on the work of Ma *et al.* (2018).

Elements on the material surface are assigned with a random local pitting parameter $\lambda_e$ value, with values in the interval of 0 and 1, according to a standard Weibull distribution. The Weibull distribution probability density function (PDF), $f(x)$, is defined as:

$$f(x:\ \psi,\ \gamma) = \begin{cases} \frac{\gamma}{\psi}\left(\frac{x}{\psi}\right)^{\gamma-1} e^{-(x/\psi)^{\gamma}} & x \geq 0 \\ 0 & x < 0 \end{cases}, \tag{7}$$

where $\gamma$ and $\psi$ are dimensionless parameters of the PDF, which determines the uniformity of the corrosion process and requires calibration based on experimental data.

In the present work, the stress corrosion model proposed by Gastaldi *et al.* (2011) based on the work of Costa *et al.* (2008) is extended by using a nonlocal integral formulation. The evolution law of the stress corrosion damage parameter is given as:

$$\frac{dD_{sc}}{dt} = \left(\frac{S\,\sigma_{eq}^*}{1-D_{sc}}\right)^R, \text{ when } \sigma_{eq}^* \geq \sigma_{th} > 0, \tag{8}$$

$$\frac{dD_{sc}}{dt} = 0, \text{ when } \sigma_{eq}^* < \sigma_{th} \tag{9}$$

where, $\sigma_{th}$ (MPa) represents a threshold value below which the stress corrosion process does not occur. Many factors must be taken into account when setting the value of $\sigma_{th}$, for example material composition and metallurgical conditions, as well as the corrosive environment; $S$, in units of $\mathrm{mm}^2\mathrm{h}^{-0.5}\mathrm{N}^{-1}$, and $R$ are constants related to the kinetics of the stress corrosion process depending on the corrosive environment and requires calibration based on experimental data; $\sigma_{eq}^*$ is a non-local averaging equivalent stress of a material point with the position vector **x**, which represents a measure for the internal stress driving the stress corrosion process and is calculated as:

$$\sigma_{eq}^*(x) = \int_V \alpha(x,y)\, \sigma_{eq}(y) dV, \tag{10}$$

where $\sigma_{eq}$ is the local equivalent stress, Von Mises stress in this case, of a material point with the position vector **y** in the influencing zone of the material point **x**. The non-local averaging approach used for equivalent stress is the same used for the pitting parameter, based on the work of Ma *et al.* (2018). It is possible to note from the previous equations that stress corrosion only occurs when the non-local averaging equivalent stress $\sigma_{eq}^*$ exceeds the value of $\sigma_{th}$ (MPa) and becomes more relevant as the stresses rise due to corrosion and deformation.

Corrosion is only allowed to occur on surface elements, which are in direct contact with the corrosion environment. When the overall damage parameter $D$ of one element reaches the critical value equal to 0.999 the element is removed from the FE mesh. After damaged element is deleted from the FE mesh, the material surface morphology is updated. In order to maintain the pitting corrosion process within the simulation, as the material surface morphology is updated, the bordering elements have their pitting parameter scaled, as proposed by Grogan *et al.* (2011), according to Eq. (11):

$$\lambda'_e = \beta\, \lambda_e, \tag{11}$$

where, $\lambda'_e$ is the scaled local pitting parameters of bordering elements, $\lambda_e$ is the value of the local pitting parameter of the removed element and $\beta$ is a dimensionless parameter that controls the pit growth within the FE analysis, which must be calibrated based on experimental data.

### 2.5 Model calibration

The mechanical behavior of uncorroded annealed Mg WE43 wires is simulated based on the results of the mechanical characterization experiments described in section 2.2, which results are presented in Table 1. The material behavior is assumed to be elastic-plastic, with linear and isotropic elasticity described through Modulus of Elasticity and Poisson's ratio ($\upsilon = 0.3$), while plasticity is modelled using Von Mises plasticity with isotropic hardening.

The pitting corrosion model parameters, $k_p$ , $\gamma$ and $\beta$ are calibrated iteratively on the basis of the results of corrosion experiments 1 and 2 presented in section 2.3, until a good fitting between simulation and experimental results is reached. A good fitting between FE model and experimental data is achieved when the simulated mass loss versus corrosion time curve corresponds qualitatively, the trend, and quantitatively, average corrosion rate, to the results obtained from corrosion experiment 1. Also, the model should be able to capture the reduction in material mechanical properties observed from corrosion experiment 2. Corrosion experiment 1 is simulated in a single step analysis, in which the surface of unloaded magnesium wire samples is allowed to corrode. The overall sample mass loss is calculated through the sum of corrosion parameter values of all model elements. Experiment 2, on the other hand, is simulated in two step analysis, in which the first step corresponds to the corrosion phase and the second step corresponds to the tensile testing of the specimen post corrosion.

The coupled pitting and stress corrosion model parameters were calibrated based on the premise that the stress cracking corrosion does not increase corrosion rate, but works by redistributing the corrosion patterner on specimen surface (Oppeel, 2015). The stress threshold of the phenomenon of stress cracking corrosion was set at 121 MPa, 50% of Yield Stress, as reported in the literature by different authors (Atrens *et al*., 2011; Gastaldi *et al.*, 2011). The influence of stress corrosion on the mechanical properties was evaluated through the simulation of a "Corrosion to Fracture" testing, as proposed by Grogan *et al*. (2011). This testing is simulated in a single step analysis, in which the surface of a constant loaded magnesium wire sample is allowed to corrode until its fracture.

The cross section of the simulation specimens is the same as the wires used in the experiments, Ø0.84 mm with the total length of the specimen corresponding to the distance between the grips of the tensile tester for experiment 2 (50 mm). The simulation part is meshed with 104244 reduced integration eight-node linear brick (C3D8R) elements.

## 3. Results

### 3.1 Mechanical characterization

The results of the mechanical characterization tensile testing are shown in Figure 2, in the form of stress–strain curves, and in Table 1, in the form of average values for Modulus of Elasticity, Yield Strength, UTS and elongation at break, for both as drawn an annealed condition.

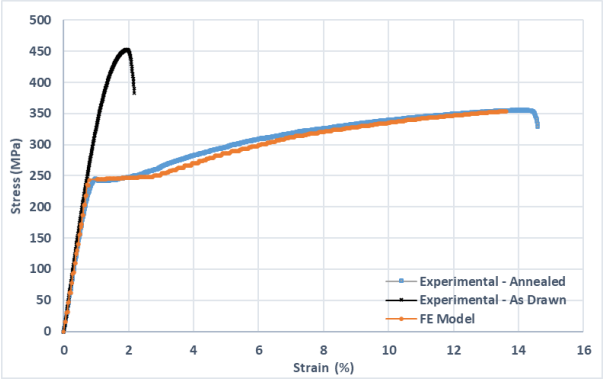


Figure 2 – Average stress-strain curves from tensile testing of wire specimens, for both As drawn and Annealed conditions. The FE model results are also shown for comparison purposes.

As can be seen from Figure 2 that the annealing process has a large impact on the mechanical properties of WE43 alloy. An increase of 5.6 times was noted for the elongation at break, with a comprise of 21.5% of reduction in UTS. The annealed condition presented a better compromise between mechanical resistance and ductility, being adopted as the thermomechanical condition for further experiments and simulation. Thus, the as drawn condition was no longer used.

Table 1 – Average mechanical properties for both As drawn and Annealed wire specimens (n=3).

| Thermal Condition | Modulus of Elasticity (GPa) | UTS (MPa) | Yield Stress (MPa) | Elongation at break (%) |
|---|---|---|---|---|
| **As Drawn** | 35.6 ± 2.0 | 454.4 ± 8.3 | 394.9 ± 10.2 | 2.20 ± 0.02 |
| **Annealed** | 31.5 ± 0.6 | 356.7 ± 2.4 | 245.9 ± 8.5 | 14.7 ± 0.2 |

### 3.2 Corrosion testing

The results of corrosion testing experiment 1, obtained from the volume of hydrogen gas evolved are shown in Figure 3. The specimens presented a high corrosion rate in the first 12h of exposure, which quickly decreased to a steady rate of mass loss, corroding by an average of 34.3% in a period of 168h, which represents an average corrosion rate of 0.080 mg $cm^2h^{-1}$.

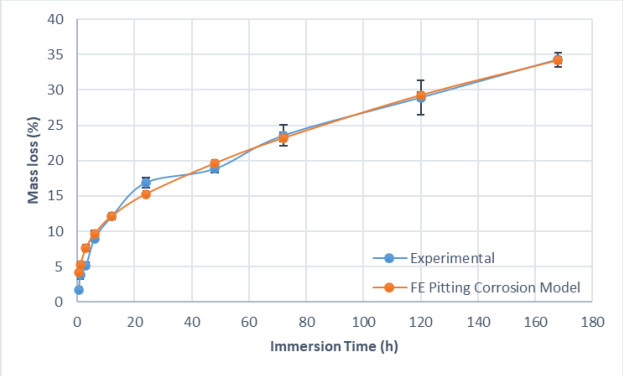


Figure 3 – Mass loss versus corrosion time from corrosion experiment 1. The FE pitting corrosion model results are also shown for comparison purposes. Error bars represent a single standard deviation from the mean (n = 3).

The results of corrosion testing experiment 2 are presented in Figure 4 in the form of UTS (a) and Elongation at Break (b) versus mass loss plot. Tensile testing data for different corrosion times were used to obtain the tensile stress–strain curves and to calculate the UTS and elongation at break, taken as representants of structural integrity loss. The results were then combined with results from experiment 1, converting the data from corrosion time to mass loss. As demonstrated in Figure 4 an increase in mass loss results in a reduction in both the UTS and in the Elongation at Break. For both mechanical characteristics, the reduction presents good linearity with mass loss, with 34.3% of corrosion resulting in 62.2% and 93.2% decrease in UTS ($R^2 = 0.95$) and in Elongation at Break ($R^2 = 0.89$) respectively.

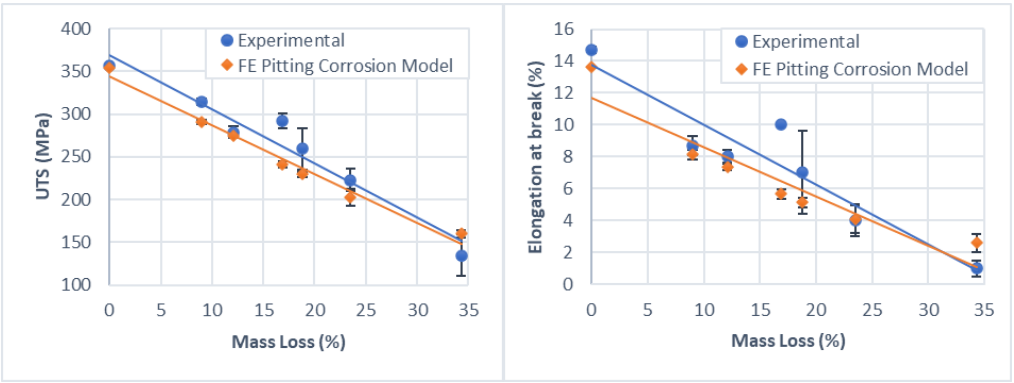


Figure 4 – Reduction in material UTS (MPA) and Elongation at Break (%) due to degradation, based on the results of experiment 2. The FE pitting corrosion model results are also shown as comparison. Error bars represent a single standard deviation from the mean (n = 3).

### 3.3 Model calibration

Figure 2 presents the stress-strain curve from FE model simulation and from mechanical characterization tensile testing. It is possible to note that the FE model was able to properly simulated the elastic-plastic behavior of the annealed WE43 magnesium alloy.

The pitting corrosion model were successfully implemented and calibrated on the basis of the results of corrosion experiments 1 and 2. The iterative calibration procedure required two calibration stages.

The first stage aimed the calibration of parameters $\gamma$ and $\beta$ focusing on the reduction of mechanical properties due to corrosion, as observed on corrosion experiment 2. As discussed before, the dimensionless parameter $\gamma$ is related to the Weibull distribution and controls the uniformity of the corrosion process on material surface.

Figure 5 illustrates the difference in the distribution of local pitting parameter, $\lambda_e$, for different values of $\gamma$. High values of $\gamma$ leads to faster and more homogenous corrosion. The non-local averaging method for the pitting parameter has a huge impact on pitting distribution, as can be seen in Figure 5. The dimensionless parameter $\beta$ controls the pitting penetration rate within the specimen, where lower values for $\beta$ leads to a more superficial corrosion patterner.

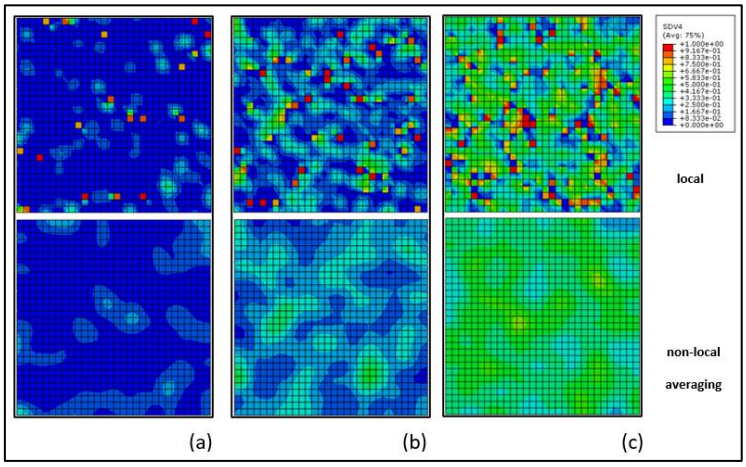


Figure 5 – Influence of different values for γ on the distribution of local pitting parameters, $\lambda_e$ (upper part) and the effect of application of non-local averaging method (lower part); (a) γ = 0.1, (b) γ = 0.4 e (c) γ = 0.9.

The second calibration stage aimed the calibration of parameter $k_p$, for the chosen set of parameters $\gamma$ and $\beta$, focusing on the corrosion trend and corrosion rate observed on corrosion experiment 1. The kinetic parameter $k_p$ is intrinsically related to the corrosion process velocity. While on the literature all magnesium pitting corrosion models available adopt a constant corrosion kinetic parameter, the present work introduced a variable corrosion kinetic parameter as a function of corrosion time, thus better representing the variable nature of corrosion rate of different magnesium alloys.

The calibrated parameters for corrosion pitting model are presented on Table 2. After the final calibrated model parameters was set, each simulation was run two more times, with different seeds of Weibull distribution, resulting in additional two different corrosion patterners. The final simulation results presented in Figure 3 and Figure 4 are the mean and the single standard deviation from mean, of the tree simulations.

Table 2 - Calibrated parameters of pitting corrosion model.

| $\gamma$ | $\beta$ | $k_p$ (h$^{-1}$) |
|---|---|---|
| 0.4 | 0.8 | $0.3125\ t^{-0.68}$ * |
| * $t$ denotes corrosion time in units of h. | | |

As can be seen from Figure 3, the calibrated pitting corrosion model can accurately represent the variable corrosion rate observed on corrosion experiment 1, as well as, provide the same average corrosion rate found experimentally. It was only possibly due to the introduction of a variable corrosion kinetic parameter, as discussed before. Also, from Figure 4 it is possible to note that the pitting corrosion model can accurately capture the linear reduction in material structural integrity, represented in the form of UTS and Elongation at break, observed from corrosion experiment 2. Figure 6 shows the evolution of the corrosion process as well as the damage parameter throughout the surface of simulation specimen as a function of time. It can be observed that a pitting-like corrosion surface is simulated by the FE model.

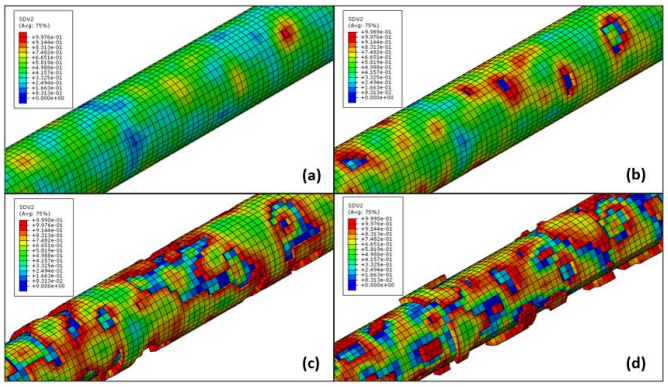


Figure 6 - Evolution of the corrosion process throughout the surface of simulation specimen as a function of time - pitting corrosion model. (a) t = 24h, (b) t = 48h, (c) t = 96h e (d) t =168h.

The coupled pitting corrosion and stress corrosion model parameters $S$ and $R$ were calibrated in a single stage calibration procedure. The parameters calibration focused on the average corrosion rate of the specimen of 34.3% over a period of 168 h, at a constant load of 125 MPa, just above the stress cracking corrosion threshold. The parameter $f$ was set at $f = 0.5$ for convenience. The calibrate values were 2.0 and 0.0006 $\mathrm{mm^2 h^{-0.5} N^{-1}}$, for $R$ and $S$ respectively.

Figure 7 illustrates the results of Corrosion to Fracture experiment simulations, for two level of loads and three proportions between the pitting corrosion model and the stress corrosion model. It is possible to note that both mechanisms are able to capture the reduction in mass loss at fracture for an increased level of tension, as reported in the literature (Grogan *et al.* 2011). At the calibration point, 125 MPa, the reduction in mass loss at fracture difference between the pitting corrosion model (*f= 0*) and the multi-mechanism model (*f=0.5*) was only 2.6%. On the other hand, for an increased load, 185 MPa, in which the stress corrosion mechanism became more important than the pitting corrosion mechanism, an increase in the mass loss at fracture of 4.7% was observed, which suggests that the stress corrosion mechanism led to a more homogenous corrosion patterner.

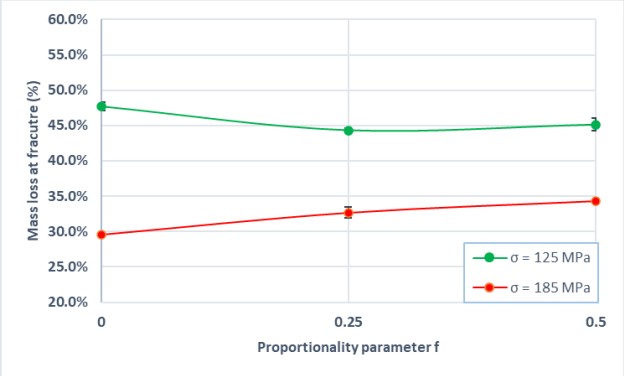


Figure 7 - Corrosion to fracture experiment simulation for two levels of constant tension. Error bars represent a single standard deviation from the mean (n = 3).

## 4. DISCUSSION

### 4.1 Mechanical characterization and corrosion testing

The results of uniaxial tensile testing for both as drawn and annealed WE43 alloy wires, Figure 2, are in accordance with the findings of by Griebel *et al.* (2018) and Maier *et al.* (2015), in similar material geometry and thermomechanical processing conditions. Different values for UTS and elongation at break have been reported for different specimen geometries, metallurgical conditions and thermal treatment, which suggests that WE43 alloy mechanical properties can be largely tuned for different applications (Boland et al., 2018; Liu et al., 2014).

Regarding the corrosion testing experiment 1, the specimens presented an average corrosion rate of 0.080 $\mathrm{mg\ cm^2 h^{-1}}$ over a period of 168h, with high corrosion rate in the first 12h of exposure, Figure 3. Qualitatively, the variable corrosion rate is in accordance with the findings of Ascencio *et al.* (2015) and may be explained by the formation of an oxide layer on material surface, which slows down the corrosion process corrosion (Zheng *et al.*, 2014). The average corrosion rate experimentally determined is within the range reported in the literature, which ranges from 0.011 $\mathrm{mg\ cm^2 h^{-1}}$ (Galvin *et al.*, 2017) to 0.89875 $\mathrm{mg\ cm^2 h^{-1}}$ (Boland *et al.*, 2018). The quite broad range found in the literature is an indication that

the corrosion rate is highly depedent on surface finishing, specimen geometry and corrosion electrolyte. Regarding corrosion testing 2, the linear reduction on mechanical properties due to corrosion also have been reported for other authors (Galvin *et al.*, 2017; Maier *et al.*, 2015).

### 4.2 Model calibration

The pitting corrosion model has been successfully calibrated to accurately capture both the linear mechanical reduction in specimen resistance, in the form of failure strength with mass loss, Figure 4, as well as the non-linear corrosion behavior of magnesium WE43, observed experimentally, Figure 5. The introduction of a variable corrosion kinetic parameter on the pitting corrosion model adds an extra level of possibilities regarding the fit of mass loss due to corrosion plots. The difference in parameter values found in this work and reported in the literature for the WE43 magnesium alloy (Boland *et al.*, 2018 and Ma *et al.*, 2018) is an indication that the model must be recalibrated for different material and testing conditions, which is a limitation of the phenomenological approach. Although in vitro and in vivo corrosion rates vary greatly, most data in this work are presented in function of mass loss instead of immersion time, which is a better characterization of the specimen structural integrity for a given situation and may help with future data extrapolation.

Similarly, the coupled pitting and stress corrosion model has been calibrated to provide the same average corrosion rate as the pitting corrosion model over a period of 168h. Regarding the influence of stress driven corrosion, the small difference found in the experiment simulations of Corrosion to Fracture between the pitting corrosion model and the multi-mechanism corrosion model may suggests that the pitting corrosion is the main factor driven the reduction in structural integrity of the material, as proposed by Grogan *et al.* (2011). Experimental data would be necessary to verify the premise that stress corrosion cracking does not increase corrosion rate, as well as to allow the definition of an optimal proportion between both corrosion mechanism and should be included as future work.

## 5. CONCLUSIONS

In the present work a Finite Element framework was successfully implemented and calibrated based on experimental data to phenomenologically simulate the influence of corrosion on the structural integrity of biodegradable magnesium alloys. The model allows for different corrosion mechanism to be accounted for: pitting corrosion and pitting corrosion coupled with stress driven corrosion. The implemented framework adds to the literature by the introduction of a variable corrosion kinetic parameter on the pitting corrosion model and the utilization of non-local averaging methodology for stress calculation on the coupled pitting and stress driven corrosion model. The nonlocal pitting corrosion model is calibrated based on experimental data collected from in-vitro corrosion experiments and mechanical testing of magnesium WE43 alloy wire specimens. The calibrated pitting corrosion model accurately captures both the linear mechanical reduction in specimen resistance, in the form of failure strength with mass loss, as well as the non-linear corrosion behavior of magnesium WE43, observed experimentally. The influence of localized stress on corrosion patterner and its influences on the mass loss at fracture were also investigated through the multi-mechanism model and showed to be of lesser relevance, when compared to the pitting corrosion mechanism, even for loads on the magnitude of 75% of the material yield stress. The calibrated numerical framework provides an efficient tool for structural integrity evaluation of biodegradable magnesium alloys and will be used in future research on design of orthopedic implants, for example, pins, screws and plates.

## 6. REFERENCES

Agarwal, S., James, C., Brendan, D., and Swarna, J., 2016. “Biodegradable Magnesium Alloys for Orthopaedic Applications: A Review on Corrosion, Biocompatibility and Surface Modifications.” *Materials Science & Engineering C*, Vol. 68, pp. 948–63.

Ascencio, M., Pekguleryuz, M., and Omanovic, S., 2015. “An Investigation of the Corrosion Mechanisms of WE43Mg Alloy in a Modified Simulated Body Fluid Solution: The Effect of Electrolyte Renewal.” *Corrosion Science*, Vol. 91, pp. 297–310.

Atrens, A., Liu, M., and Abidin, N.I.Z., 2011. “Corrosion Mechanism Applicable to Biodegradable Magnesium Implants.” *Materials Science and Engineering B: Solid-State Materials for Advanced Technology*, Vol. 176, No. 20, pp. 1609–36.

Boland, E.L., Shirazi, R.N., Grogan, J.A., and McHugh, P.E., 2018. “Mechanical and Corrosion Testing of Magnesium WE43 Specimens for Pitting Corrosion Model Calibration.” *Advanced Engineering Materials*, Vol. 20, No. 10, pp. 1–11.

Costa-mattos, H.S., Bastos, I.N., and Gomes, J.A.C.P., 2008. “A Simple Model for Slow Strain Rate and Constant Load Corrosion Tests of Austenitic Stainless Steel in Acid Aqueous Solution Containing Sodium Chloride.” *Corrosion Science*, Vol. 50, No.10, pp. 2858–66.

Fathi, F., Ardakani, S.H, Dehaghani, P.F., and Mohammadi, S., 2017. “A Finite Strain Integral-Type Anisotropic Damage Model for Fiber-Reinforced Materials: Application in Soft Biological Tissues.” *Computer Methods in*

*Applied Mechanics and Engineering*, Vol. 322, pp. 262–95.

Galvin, E., O'Brien, D., Cummins, C. , Mac Donald, B.J., and Lally, C., 2017. "A Strain-Mediated Corrosion Model for Bioabsorbable Metallic Stents." *Acta Biomaterialia*, Vol. 55, pp. 505–17.

Gastaldi, D., Sassi, V., Petrini, L., Vedani, M., Trasatti, S., and Migliavacca, F., 2011. "Continuum Damage Model for Bioresorbable Magnesium Alloy Devices — Application to Coronary Stents." *Journal of the Mechanical Behavior of Biomedical Materials*, Vol. 4, No. 3, pp. 352–65.

Griebel, A.J., Schaffer, J.E., Hopkins, T.M., Alghalayini, A., Mkorombindo, T., Ojo, K.O., Xu, Z., Little, K.J., and Pixley, S.K., 2018. "An in Vitro and in Vivo Characterization of Fine WE43B Magnesium Wire with Varied Thermomechanical Processing Conditions." *Journal of Biomedical Materials Research - Part B Applied Biomaterials* Vol. 106, No. 5, pp. 1987–97.

Grogan, J.A., 2013. "The Mechanical Performance of Permanent and Bioabsorbable Metal Stents." National University of Ireland. http://hdl.handle.net/10379/3744. Accessed 08 September 2020.

Grogan, J.A., O'Brien, B.J., Leen, S.B., and McHugh, P.E., 2011. "A Corrosion Model for Bioabsorbable Metallic Stents." *Acta Biomaterialia*, Vol. 7. No. 9 pp. 523–33.

Kirkland, N.T., Birbilis, N., and Staiger, M.P., 2012. "Assessing the Corrosion of Biodegradable Magnesium Implants: A Critical Review of Current Methodologies and Their Limitations." *Acta Biomaterialia* Vol. 8, No. 3, pp. 925–36.

Lemaitre, J., 1985. "A Continuous Damage Mechanics Model for Ductile Fracture." *Journal of Engineering Materials and Technology* Vol. 107, pp. 83–89.

Liu, D., Ding, Y., Guo, T., Qin, X., Guo, C., Yu, S., and Lin, S., 2014. "Influence of Fine-Grain and Solid-Solution Strengthening on Mechanical Properties and in Vitro Degradation of WE43 Alloy." *Biomedical Materials (Bristol)*, Vol. 9, pp. 1-9.

Ma, S., Zhou, B., and Markert, B., 2018. "Numerical Simulation of the Tissue Differentiation and Corrosion Process of Biodegradable Magnesium Implants during Bone Fracture Healing." *ZAMM Zeitschrift Fur Angewandte Mathematik Und Mechanik*, Vol. 98, pp. 2223–38.

Maier, P., Griebel, A.J., Scheffler, O., and Schaffer, J.E., 2015. "Remaining Strength of Cold Drawn and Aged WE43 Wires after Corrosion." *European Cells and Materials*. Vol. 30, Suppl. 3, pp. 47.

Oppeel, A., 2015. "Experimental Characterisation and Finite Element Modeling of Biodegradable Magnesium Stents." Master Dissertation in Biomedical Engineering, Universiteit Gent, Ghent, Belgium. https://www.ugent.be/ea/bme/en/program/bachelor/masterthesis/oppeel-lq.pdf. Accessed 07 September 2020.

Oyane, A., Kim, H., Furuya, T., Kokubo, T., Miyazaki, T., and Nakamura, T., 2002. "Preparation and Assessment of Revised Simulated Body Fluids." *Journal of Biomedical Materials Research*, Vol. 65A, pp. 188–95.

Seitz, J., Lucas, A., and Kirschner, M., 2016. "Magnesium-Based Compression Screws : A Novelty in the Clinical Use of Implants." *JOM*, Vol. 68 (4), pp. 1177–82.

Song, G., Atrens, A., and StJohn, D., 2001. "An Hydrogen Evolution Method for the Estimation of the Corrosion Rate of Magnesium Alloys." In *Magnesium Technology 2001*, edited by John N. Hryn, 256–62. Hoboken, NJ, USA: TMS.

Song, G., and Atrens, A., 2003. "Understanding Magnesium Corrosion. A Framework for Improved Alloy Performance." *Advanced Engineering Materials* Vol. 5 (12), pp. 837–58.

Staiger, M.P., Pietak, A.M., Huadmai, J., and Dias, G., 2006. "Magnesium and Its Alloys as Orthopedic Biomaterials : A Review." *Biomaterials*, Vol. 27, pp. 1728–34.

Waizy, H., Diekmann, J., Weizbauer, A., Reifenrath, J., Bartsch, I., and Neubert, V., 2014. "In Vivo Study of a Biodegradable Orthopedic Screw (MgYREZr-Alloy) in a Rabbit Model for up to 12 Months." *Journal of Biomaterials Applications*, Vol. 28 (5), pp. 667–75.

Yang, L., and Zhang, E., 2009. "Biocorrosion Behavior of Magnesium Alloy in Different Simulated Fluids for Biomedical Application." *Materials Science & Engineering C*, Vol. 29 (5), pp.1691–96.

Zheng, Y.F., Gu, X.N., and Witte, F., 2014. "Biodegradable Metals." *Materials Science and Engineering: R: Reports*, Vol. 77, pp. 1–34.

## 7. RESPONSIBILITY NOTICE

The authors are the only responsible for the printed material included in this paper.